ELSEVIER

Earth and Planetary Science Letters 125 (1994) 17–37

EPSL

Isotopic constraints on the production rates, crystallisation histories and residence times of pre-caldera silicic magmas, Long Valley, California

Gareth R. Davies [a,1], Alex N. Halliday [a], Gail A. Mahood [b], Chris M. Hall [a]

[a] *Department of Geological Sciences, University of Michigan, Ann Arbor, MI 48109-1063, USA*
[b] *Department of Geological and Environmental Sciences, Stanford University, Stanford, CA 94305-2115, USA*

Received 3 April 1992; revision accepted 19 May 1994

Abstract

Pre-caldera high-silica rhyolites of Glass Mountain, California erupted episodically from 2.1 Ma until the catastrophic eruption of the Bishop Tuff at 0.74 Ma. The lavas are extremely evolved, with Rb/Sr ratios between 128 to 3640, the latter being the highest recorded from a volcanic rock. Glass separates from pre-1.2 Ma lavas define two geographically controlled Rb-Sr isochrons. Lavas adjacent to the current caldera rim define an isochron age of 2.047 ± 0.013 Ma with an initial ratio of 0.7063 ± 2, and lavas more distant from the caldera define an isochron of 1.894 ± 0.013 Ma with the same initial ratio. The isochrons are consistent with the magmas forming within 26 ka, which implies a minimum magma production rate of 0.75×10^{-3} km^3/yr over this period. New ^{40}Ar-^{39}Ar ages on sanidine and biotite have established that lavas defining each isochron were erupted over a long time interval, the isochron ages being up to 360 ka older than the youngest eruption age.

Rb-Sr isotope data are reported for minerals from three lavas with eruption ages of 1.990 ± 0.012, 1.866 ± 0.014 and 1.686 ± 0.011 Ma. Petrographically early apatite inclusions in biotite and biotite inclusions in feldspar and quartz have glass–mineral Rb-Sr ages that are indistinguishable from the relevant regional isochron. Sr diffusion in feldspar is slow at the magmatic temperatures inferred for Glass Mountain rhyolites ($\sim$ 700°C) such that over 0.5 Ma the cores of large feldspars ($>$ 1 mm) will retain $>$ 99.9% of their original Sr. The cores of sanidine and plagioclase yield glass–mineral ages that are up to 300 ka older than eruption ages. Feldspar rim ages for two samples are indistinguishable from eruption ages. The rims of sanidines and plagioclases from the third sample are 110 and 280 ka older than the eruption age and 180 and 20 ka younger than the cores. These mineral age data probably reflect the combination of extended periods of mineral growth and partial isotopic exchange with the host liquid during protracted residence in a magma reservoir. However, the Ar and Sr isotopic data for biotite phenocrysts are consistent with the presence of a significant component that is recycled from earlier magmatic pulses.

Due to the extreme Rb/Sr ratios of the rocks and minerals it is possible to very precisely resolve the time difference between the formation of different phases, assuming that they crystallised from the same host magmas (e.g., $T_{\text{plagioclase}} - T_{\text{Fe-Ti oxide}} = 6.8 \pm 0.1$ ka) and the maximum time taken to form a phase (e.g., $T_{\text{plagioclase core}} - T_{\text{plagioclase rim}} = 32.3 \pm 0.2$ ka). The timescale for mineral growth is shorter in the chemically more evolved and

[RvdV]

[1] Now at: Faculteit der Aardwetenschappen, Vrije Universiteit, 1081 HV Amsterdam, The Netherlands

Elsevier Science B.V.
SSDI 0012-821X(94)00120-N

crystal-poor lavas, consistent with these magmas having resided at higher levels in the magma chamber with shorter residence times and being more liable to extrusion. By using mineral inclusion relationships, average mineral growth rates are estimated to be between 7×10^{-13} and 8×10^{-14} cm/s. These values are significantly lower than those measured in basaltic systems and probably reflect a combination of the slow cooling rate of the Glass Mountain magma chamber(s) and the highly polymerised nature of high-silica magmas.

1. Introduction

Rates of magma differentiation and residence times of silicic magmas in crustal magma chambers have been estimated from observations of the volume and periodicity of eruptive products at individual volcanic centres [1,2] and by modelling the thermal and fluid dynamic properties of magmas [3]. Rb/Sr ratios of many high-silica rhyolites are sufficiently high ($> 10^3$) that the Sr isotope compositions can be used to place direct limits on the time span of magma differentiation [4,5]. In certain instances, periods of the order of 10^3 yr can be accurately measured with current techniques. Furthermore, if the phenocrysts are cogenetic with their host glasses, the timing of crystal growth can be determined even more precisely and growth rates can be deduced from core–rim disequilibria, provided re-equilibration is slow relative to change in Sr isotope composition by in-situ decay. Current estimates of crystal growth rates, which range from 10^{-6} to 10^{-11} cm/s, have been determined experimentally, from crystal size distributions and from the the observation of rapidly cooling 'basaltic' lava lakes [6]. To date, there is little information about the growth rates of minerals in silicic systems. In this paper, the Rb-Sr isotope systematics of pristine high-silica rhyolite lavas from Glass Mountain, California are used to place limits on the timing of differentiation, the production rates of the magmas, phenocryst growth rates and the residence time of magmas prior to eruption.

2. Glass Mountain Lavas

Glass Mountain is located on the northeastern margin of the Long Valley caldera in east-central California and consists of over 50 km^3 of high-silica rhyolite lavas and pyroclastic deposits (Fig. 1) [7]. There are at least 50 lava flows, many of which locally contain pristine glass. Individual lava domes have volumes between 0.1 and 5 km^3 (Fig. 1). Rhyolitic volcanism began at 2.1 Ma and continued episodically until the caldera-forming eruption of the Bishop Tuff at 0.74 Ma [7]. The lavas of Glass Mountain are very evolved [7,8], with low phenocryst contents of typically less than 3% and comprising quartz, sanidine, plagioclase and biotite. Lavas erupted prior to 1.2 Ma tend to be smaller in volume with more evolved and varied compositions than the younger Glass Mountain lavas, which are slightly less evolved than the earliest Bishop Tuff. The Nd isotope compositions are more radiogenic in the younger (post-1.2 Ma) lavas, marking the formation of a new magma system that eventually produced the Bishop Tuff magma 500 ka later [4,5,8,9].

In an earlier study of Glass Mountain rhyolites, Halliday et al. [4] reported two Rb-Sr isochrons among the pre-1.2 Ma lavas that were delimited by the geographical distribution of the lavas. A 2.09 ± 0.06 Ma isochron was defined by the lavas closest to the present caldera, whereas a 1.90 ± 0.02 Ma was determined for lavas further away. Halliday et al. [4] argued that the preservation of these isochronal relationships in magmas erupted as lavas at a much later time (as late as 1.35 Ma [7]) implied that magma formation occurred in two discrete events and that the magmas subsequently remained in a stable, stratified state for up to 700 ka. Christensen and DePaolo [5] also argued for a prolonged evolution for the Bishop Tuff magma system on the basis of Sr isotope differences between sections of the Bishop Tuff and Sr isotope disequilibrium between feldspars and their host glasses. Sparks et al. [10] pointed out that there are thermal constraints imposed upon the state of a magma chamber if it

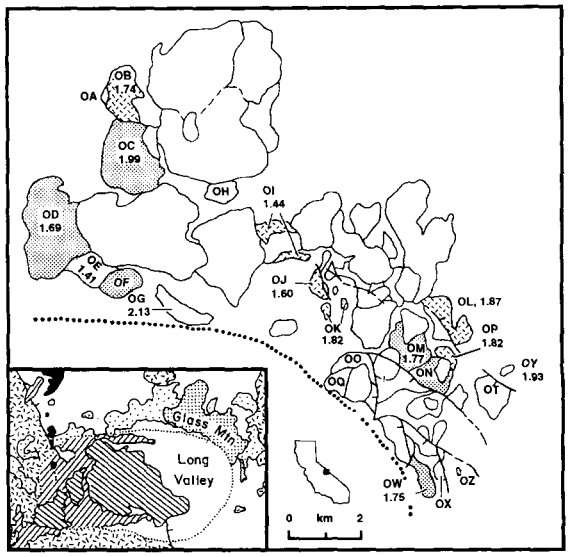

Fig. 1. Sketch map of Glass Mountain modified from Metz and Bailey [39]. Prefix 'O' is for older, pre-1.2 Ma lavas (individual flow units distinguished by letters). Unmarked area on map represents tuffs of Glass Mountain and Bishop Tuff together with caldera lake sediments and Recent surficial deposits. Inner Lavas which lie on Rb-Sr isochron of age 2.047 ± 0.013 Ma are represented by stipple pattern. Outer Lavas which lie on Rb-Sr isochron of age 1.894 ± 0.013 Ma are represented by dashed pattern.

were to exist for 700 ka and reinterpreted the data in terms of remelting recently crystallised granites deep within the crust. Mahood [11] modified this second model and proposed remelting or 'defrosting' of the crystallised margins of the high-level Long Valley magma chamber(s) to explain the Rb-Sr isochrons. Halliday [12] pointed out the physical problems of repeatedly remelting a source or magma chamber and still preserving a Rb-Sr isochron defined by low-Sr liquids.

The aims of this study of the Glass Mountain Older Lavas were to confirm that the differences between the Rb-Sr isochrons and K-Ar eruptive ages were valid [4,7,12], test the hypothesis of protracted magma residence by using the Rb-Sr isotope systematics of minerals to constrain the crystallisation history and to provide precise magma production and crystal growth rates for high-silica rhyolites.

3. Petrography

Samples from three lavas (OD, OC and OL of [8]) were examined in detail. Quartz, biotite, sanidine and plagioclase are the dominant phenocryst phases. Small euhedral biotites (< 0.1 mm) are included as cores to quartz but are found throughout sanidine and plagioclase grains. Apatite, zircon, Fe-Ti oxides and allanite are common inclusions in biotite but are rare in other phases. Plagioclase inclusions are common in sanidine and both feldspars are found included in quartz. Biotite contains neither quartz nor feldspar inclusions, implying that in the studied samples biotite crystallised early and quartz later. Crystallisation of minor phases appears to have begun early; the presence of large discrete grains in some lavas [8] implies that their crystallisation was long-lived. Feldspar phenocrysts are euhedral, indicating equilibrium crystallisation from a melt with no evidence of resorption.

Microprobe analyses of hand-picked separates demonstrate that the phenocrysts are only modestly zoned in major element composition [8,13]. However, both plagioclase and sanidine invariably have a thin (ca. 0.1 mm) overgrowth of sodic plagioclase. Crushing and sieving of samples tended to detach part or all of the overgrowths. TEM studies demonstrate that this overgrowth is poorly crystalline and probably formed under conditions of high vapour pressure [14]. Similar overgrowths are found throughout the Bishop Tuff such that in hand specimen many feldspars appear altered despite having a gem-quality core [13,14]. Typically feldspar grains are 1–5 mm in diameter, although larger feldspar grains with a maximum size of 1.0 cm were recorded in each sample ($< 0.1\%$ of the population). Microdrilling was carried out on the largest (> 5 mm) grains that retained the sodic plagioclase overgrowth. The representative mineral analyses of all phases are reported elsewhere [8].

Some of the Glass Mountain lavas contain a sparse xenocrystic population probably derived from local basement rocks [8]. Partially altered albite and Ca-poor anorthoclase were observed in bulk separates from samples OC and OL ($< 0.1\%$ of each of the feldspar populations). Very rare

pale brown biotites were observed in sample OC (< 0.01% of biotite population). These xenocrysts have ragged or rounded margins and were excluded from the analysed material during hand-picking. Microprobe analyses of the xenocrystic minerals generally yielded poor totals, confirming the petrographic observation that they were partially altered. With the exception of the rare xenocrysts, biotite compositions are homogeneous in the three studied samples [8,13]. Sanidine and plagioclase compositions were also found to be relatively homogeneous. For example, the orthoclase content of the three sanidine populations studied here varied between Or_{52} and Or_{61} ($N >$ 15 for each sample [13]).

4. Techniques

After hand-picking, the mineral and glass samples were repeatedly cleaned by ultrasonic agitation in acetone and water. Multiple quartz fractions were separated according to their inclusion content. A composite of biotite inclusions was extracted from a mixed quartz–sanidine–plagioclase population of OD. Similarly two apatite com-

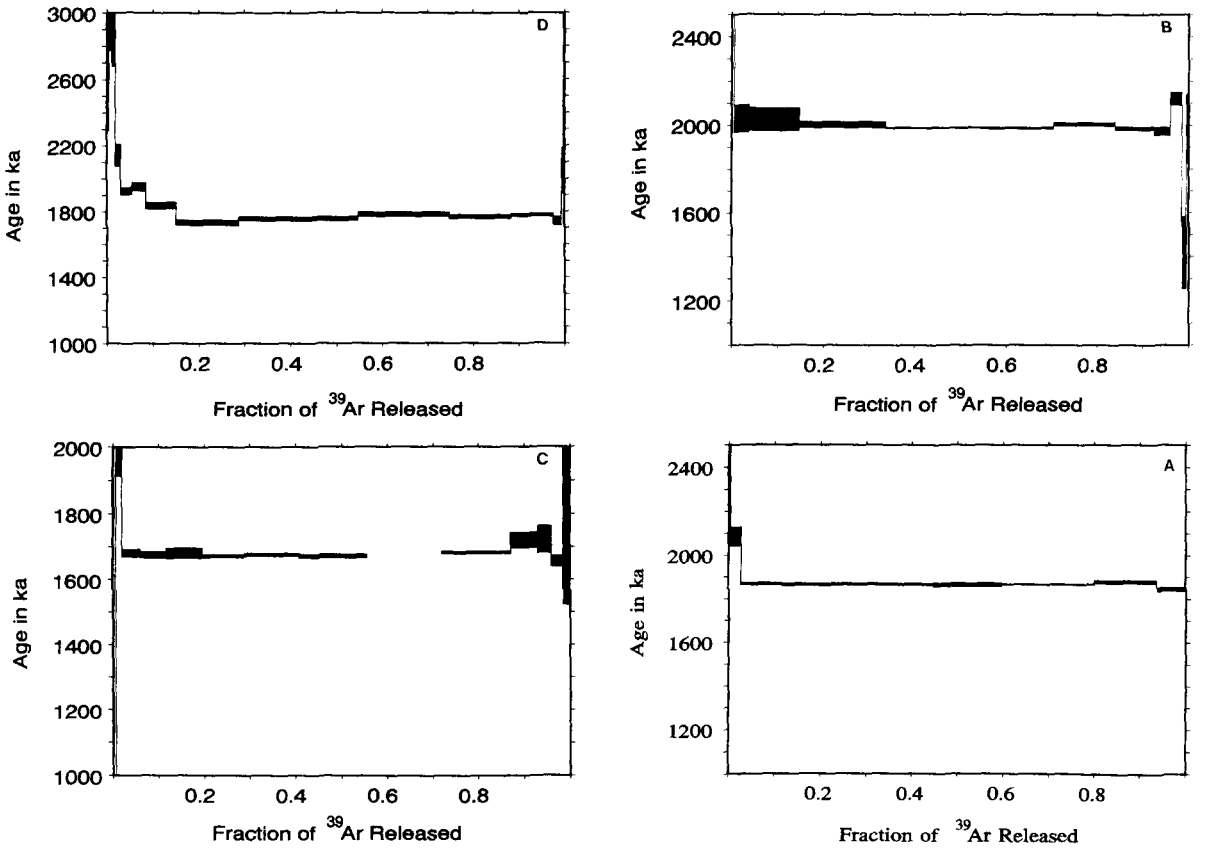

Fig. 2. ^{40}Ar-^{39}Ar step release spectra from (A) sanidine composite from lava OD. Total degas age is 1.704 ± 0.016 Ma. The data yield a plateau age of 1.691 ± 0.014 Ma on 83.2% of the gas and an ^{36}Ar/^{40}Ar vs. ^{39}Ar/^{40}Ar isochron age of 1.686 ± 0.011 Ma. One step was not analysed due to an electrical malfunction in the magnet power supply. The gas fraction became very fractionated before analysis was possible but the volume of gas is known. (B) Biotite composite from lava OD. Total degas age is 1.815 ± 0.019 Ma with a significant inherited argon component. The data yield an ^{36}Ar/^{40}Ar vs. ^{39}Ar/^{40}Ar age of 1.688 ± 0.038 Ma. (C) Sanidine composite from lava OC. Total degas age is 1.976 ± 0.091 Ma. The data yield a plateau age of 1.999 ± 015 Ma on 95.4% of the gas and an isochron age of 1.990 ± 0.012 Ma. (D) Sanidine composite from lava OL. Total degas age is 1.895 ± 0.017 Ma. The data yield a plateau age of 1.867 ± 0.005 Ma on 77.4% of the gas and an isochron age of 1.866 ± 0.014 Ma.

Table 1
Ar data

Sample	Total Gas Age (Ma)	+/-	Plateau Age (Ma)	+/-	% ^{39}Ar in plateau	Isochron n	% ^{39}Ar in isochron	MSWD	$(^{40}Ar/^{36}Ar)_i$	+/-	Isochron Age (Ma)	+/-
OD												
Biotite Step-heat	1.82	0.02				18	100	6.4	306.1	2.6	1.69	0.04
Sanidine Step-heat	1.704	0.016	1.691	0.014	83.2	11	83.2	1.0	295.1	1.2	1.686	0.011
Sanidine Laser	1.72	0.03				12		2.7	297	33	1.71	0.06
All Sanidine						23		2.0	295	1.5	1.687	0.012
OC												
Sanidine Step-heat	1.98	0.09	1.999	0.015	95.4	8	95.4	1.1	296	2.9	1.990	0.012
Sanidine Laser	2.11	0.12				12		0.5	264	109	2.2	0.4
All Sanidine						20		0.8	296.1	2.7	1.990	0.011
OL												
Sanidine Step-heat	1.895	0.017	1.867	0.005	77.4	5	77.4	0.1	297.7	2.8	1.866	0.014
Sanidine Laser	2.0	0.1				12		0.8	456	667	1.8	0.5
All Sanidine						17		0.7	299	13	1.866	0.014

posites (ten and fifteen grains) were extracted from inclusion-bearing biotites in lava OD. The reproducibility of Rb/Sr ratios over the two-year period of this study was found to be better than 0.5%, but a conservative value of 1% is used in all age calculations. Isotope analyses of feldspars were confined to the largest grains in each sample. To check for homogeneity, multiple bulk and individual feldspar grains were analysed. Bulk feldspar separates were hand-picked to ensure they did not contain translucent plagioclase overgrowths. In addition, cores and translucent overgrowths of the largest feldspar grains were sampled using a microdrill. Bulk sanidine separates for ^{40}Ar-^{39}Ar analysis were prepared as above and each separate split 10% and 90%, for laser-probe and step-heating respectively.

Sr-Nd-Pb isotope analyses were carried out at the University of Michigan following standard procedures [4]. A Sr blank was measured with every eleven samples. Nine Sr blank determinations ranged between 45 and 87 pg and yielded ^{87}Sr/^{86}Sr ratios of 0.7156–0.7164. The Sr isotope ratios of glasses were determined on relatively large samples (50–75 mg). Blank corrections were $< 0.3\%$ and were ignored for all samples except OL, for which a correction of 1.7% was applied. All isotopic measurements were performed on V.G. Sector multicollector thermal ionisation mass spectrometers. The average ^{87}Sr/^{86}Sr for NIST SRM 987 was 0.710259 ± 12 ($N > 100$) and the average ^{143}Nd/^{144}Nd for the La Jolla Nd standard was 0.511857 ± 6 ($N > 100$). All Pb isotope ratios were normalised using NIST SRM 981 with a fractionation factor of 0.11%/amu.

Step-heating ^{40}Ar-^{39}Ar analyses were performed at the University of Michigan using a Mass Analyser Products 215 mass spectrometer equipped with a Faraday cup and an electron multiplier (gain $\approx$ 8000). Each step included 20 min of heating and 5 min for clean-up. Typical blanks at mass 40 were about 2×10^{-11} ml STP at 900°C and about 1.4×10^{-9} ml STP at 1700°C. The ages for all of the Michigan analyses are based upon an age of 520.4 Ma for standard hornblende MMhb-1. Laser fusion ^{40}Ar-^{39}Ar analyses were performed at the University of Toronto [15]. Ages calculated for these samples are based on an age for standard biotite 4B of 17.25 Ma, which in turn is referenced to an age of 1071 Ma for standard hornblende 3gr.

5. Isotopic data

5.1. ^{40}Ar-^{39}Ar ages

The ^{40}Ar-^{39}Ar results are presented in Fig. 2 and summarised in Table 1 (2σ errors are reported throughout this paper). The plateau ages and the step-heating and laser total gas ages are in agreement, indicating little excess ^{40}Ar in the sanidines. All isochrons for plateau fractions are compatible with initial Ar with an atmospheric isotopic composition (Table 1). For all three samples studied (OC, OD and OL), the laser-generated single crystal ages and the plateau fractions of the step-heating runs define an isochron (Table 1). The best estimates for the eruption ages of these units are 1.990 ± 0.012 Ma (OC), 1.686 ± 0.011 Ma (OD) and 1.867 ± 0.005 Ma (OL). These ages are consistent with the available field relationships, which demonstrate that the rhyolite dome OC is older than adjacent domes (e.g., OB = 1.74 Ma).

The biotite separate from OD yields a total fusion age which is significantly higher than that of the coexisting sanidine. The biotite's age spectrum is saddle-shaped, with a minimum at about 1.74 Ma, significantly older than the 1.69 Ma age for the sanidine. However, an isochron fit through all eighteen biotite fractions yields an apparent age of 1.688 ± 0.038 Ma, which is indistinguishable from the coexisting sanidine results. The apparent initial ^{40}Ar/^{36}Ar ratio was 306 ± 3 in the biotite, indicating that the mineral received a non-atmospheric component. The concordancy between the sanidine laser fusion ages (where many different grains are analysed individually) and the step-heating results for sanidine and biotite from the same rock provide powerful evidence against post-eruptive argon loss. The agreement with field relationships provides confirmation that these new ^{40}Ar/^{39}Ar ages accurately date the eruption of the lavas when the minerals last cooled below their Ar blocking tem-

peratures. Nevertheless, there is evidence for a slight excess Ar component in the biotites, consistent with the Rb-Sr evidence presented below indicating that some biotites may be recycled from earlier pulses of magma. In a previous study [7] K-Ar ages were reported for glass and sanidine from the same lava flows. Sample OC yields an age of 1.990 ± 0.012 Ma within error of the previous result (1.92 ± 0.10 Ma). The new analysis of sample OL (1.867 ± 0.005 Ma) is also within the uncertainties reported previously (1.56 and 1.63 ± 0.30 Ma). In contrast, sample OD yields a plateau age of 1.686 ± 0.011 Ma, which is significantly older than the previously reported ages of 1.35 ± 0.20 Ma from a sanidine composite and 1.33 ± 0.20 Ma from the felsite.

5.2. Glass Rb-Sr isotope data

Rb/Sr ratios of rhyolite glasses from the Older Lavas at Glass Mountain range from 127.6 to 3637 (Table 2). The Rb contents of the rhyolite glasses are not exceptionally high (165–313 ppm), but the Sr contents are generally below 1 ppm. Sample OL has the lowest Sr content recorded from a volcanic glass (0.069 ppm) and the highest Rb/Sr ratio (> 3600), equivalent to $^{87}Rb/^{86}Sr = 11{,}000$. The radiogenic Sr and low Sr contents make these samples extremely sensitive to any form of contamination. Despite the young age of the Glass Mountain lavas (< 2.1 Ma) the large range in Rb/Sr ratios result in variable present-day $^{87}Sr/^{86}Sr$ (0.7173–1.0012). The Sr isotope ratios calculated for the time of eruption determined by Ar dating ($^{87}Sr/^{86}Sr_e$)are also variable, ranging from 0.7059 to 0.7196. There is no simple temporal relationship between the age of the lavas and $^{87}Sr/^{86}Sr_e$ (Table 2 [4]).

5.3. Mineral Rb-Sr isotope data

Mineral phases from different samples have large variations in present-day Sr isotope compositions (e.g., bulk sanidine = 0.7078–0.7179 (Table 3)). Duplicate Sr isotope analyses of sanidine and plagioclase composites and individual grains free of overgrowths from sample OD are within analytical error, which implies that the feldspars represent single populations (Table 3). A precise $^{87}Sr/^{86}Sr$ profile across individual feldspar grains has, so far, proved impossible owing to the relatively low Sr concentrations. Core–rim relation-

Table 2
Rb-Sr isotope data for older lavas from Glass Mountain

SAMPLE		AGE Ma[1]	Rb ppm	Sr ppm	Rb/Sr	$^{87}Rb/^{86}Sr$	$^{87}Sr/^{86}Sr$	$^{87}Sr/^{86}Sr_e$[3]
inner lavas								
OC	GLASS	1.990[2]	311.6	0.149	2087	6143	0.88389±1	0.71032
ON	GLASS	1.77	169.5	0.765	221.6	642.1	0.72484±1	0.70870
OM	GLASS	1.77	177.3	1.168	151.8	439.7	0.71883±1	0.70778
OD	GLASS	1.686[2]	288.4	2.260	127.6	369.5	0.71726±1	0.70841
OF	GLASS	?	165.2	0.726	227.5	659.5	0.72509±1	
OZ	GLASS	?	202.4	0.688	294.4	853.7	0.73079±1	
outer lavas								
OK	GLASS	1.89	184.2	0.160	1153	3366	0.79619±1	0.70585
OL	GLASS	1.867[2]	249.9	0.0687	3637	10827	1.00215±3	0.71526
OB	WR	1.74	207.1	0.105	1972	5792	0.86136±1	0.71824
OJ	GLASS	1.6	187.3	0.164	1142	3333	0.79527±1	0.71955
OI	GLASS	1.44	191.2	0.473	404.2	1173	0.73761±1	0.71363

[1] K-Ar ages from [7]; [2] ^{40}Ar-^{39}Ar ages from sanidine (see Table 1); [3] initial ratios calculated at time of eruption defined by Ar ages.

Table 3
Mineral Rb-Sr isotope data

MINERAL	Rb ppm	Sr ppm	Rb/Sr	$^{87}Rb/^{86}Sr$	$^{87}Sr/^{86}Sr$	$^{87}Sr/^{86}Sr_e$	GLASS-MIN AGE (Ma)
Sample OD							
Glass	288.4	2.260	127.6	369.5	0.717260±10	0.70841	
Biotite > 250mm	617.6	0.7111	868.5	2529	0.772402±24	0.71186	1.799 ± 0.011
Biotite 150-250mm	603.4	0.7864	767.3	2233	0.767607±26	0.71414	1.903 ± 0.012
Biotite 4mm	634.8	0.7033	902.6	2628	0.773871±18	0.71095	1.765 ± 0.010
Biotite inclusions	578.3	0.8297	697.0	2028	0.765197±22	0.71665	2.036 ± 0.013
Plagioclase bulk	10.06	49.164	0.2046	0.5920	0.706911±11	0.70690	1.975 ± 0.010
Plagioclase single	10.11	49.057	0.2062	0.5964	0.706918±12	0.70690	1.974 ± 0.010
Plagioclase single	10.16	49.664	0.2045	0.5915	0.706909±12	0.70690	1.976 ± 0.010
Plagioclase core	7.68	52.365	0.1467	0.4244	0.706843±16	0.70683	1.988 ± 0.010
Plagioclase rim	14.74	32.131	0.4587	1.328	0.706984±14	0.70695	1.965 ± 0.010
Sanidine bulk (1)	128.3	12.135	10.57	30.58	0.707819±12	0.70709	1.962 ± 0.011
Sanidine bulk (2)	129.4	12.133	10.66	30.85	0.707833±12	0.70710	1.960 ± 0.011
Sanidine bulk (3)	129.2	12.123	10.65	30.82	0.707823±12	0.70710	1.962 ± 0.011
Sanidine single	128.8	12.134	10.61	30.70	0.707825±12	0.70709	1.961 ± 0.011
Sanidine single	128.3	12.112	10.59	30.64	0.707822±12	0.70709	1.961 ± 0.011
Sanidine core	121.4	12.513	9.698	28.06	0.707719±10	0.70705	1.968 ± 0.011
Sanidine rim	25.37	17.634	1.439	4.163	0.707970±11	0.70787	1.791 ± 0.009
Quartz mix.	1.556	0.01549	100.5	290.9	0.715201±16	0.70824	
Quartz + feldspar	2.452	0.03015	81.33	235.4	0.713675±14	0.70803	
Quartz + melt inc.	1.017	0.00681	149.3	432.5	0.719026±18	0.70867	1.97 ± 0.1
Fe-Ti Oxide	2.566	1.2029	2.133	6.171	0.706753±10	0.70668	2.036 ± 0.011
Apatite	0.032	129.58	0.00025	0.00071	0.706552±10	0.70655	2.040 ± 0.010
Apatite	0.047	125.35	0.00038	0.00108	0.706553±10	0.70655	2.040 ± 0.010
Sample OC							
Glass	311.6	0.149	2087	6143	0.883892±11	0.71032	
Biotite <350mm	743.0	0.79171	938.5	2736	0.785923±25	0.70861	2.03 ± 0.02
Biotite >350mm	767.4	0.76887	998.1	2911	0.790014±19	0.70776	2.05 ± 0.021
Plagioclase bulk	19.93	3.9133	5.094	14.74	0.708052±12	0.70764	2.0206± 0.0099

Plagioclase core	15.89	4.115	3.86	11.17	0.706713±14	0.70640	2.035 ± 0.010
Plagioclase rim	21.45	3.723	5.761	16.68	0.712724±12	0.71225	1.9677± 0.0097
Sanidine bulk	136.28	1.4971	91.03	263.6	0.715782±11	0.70833	2.014 ± 0.010
Sanidine rim	144.78	1.175	123.2	356.9	0.720221±14	0.71013	1.992 ± 0.010
Sanidine core	133.53	1.834	72.81	210.8	0.712664±12	0.70671	2.033 ± 0.010
Quartz bulk	23.40	0.07292	320.9	930.9	0.735553±12	0.70925	2.004 ± 0.012
Fe-Ti oxides	5.28	0.09827	53.77	155.6	0.710026±14	0.70563	2.045 ± 0.010
Sample OL							
Glass	249.9	0.06871	3637	10827	1.00215 ±2	0.71526	
Sanidine bulk	115.7	1.155	100.2	290.1	0.717914±12	0.71023	1.8996 ± 0.0096
Sanidine core	108.7	1.452	74.83	216.7	0.714642±13	0.70890	1.9081 ± 0.0095
Sanidine rim	39.87	1.241	32.13	93.12	0.720462±14	0.71800	1.8480 ± 0.0090
Plagioclase bulk	15.59	4.605	3.39	9.801	0.708852±12	0.70859	1.9093 ± 0.0094
Plagioclase rim	19.67	4.1171	4.778	13.83	0.713923±12	0.71356	1.8770 ± 0.0092
Biotite+inclusions	411.2	9.0419	45.47	131.63	0.711502±08	0.70801	1.9136 ± 0.0095
Biotite >250mm	596.7	0.70145	850.6	2477	0.774013±14	0.70837	1.924 ± 0.013
Biotite >250mm	626.3	0.5695	1100	3207	0.786647±10	0.70167	1.991 ± 0.014
Fe-Ti Oxide	1.113	0.5166	2.154	6.234	0.707712±14	0.70755	1.9161 ± 0.0094

ships were investigated, however: Both sanidine and plagioclase core samples have less measured radiogenic $^{87}Sr/^{86}Sr$ than the bulk separates and individual grains (e.g., 0.70772 compared to 0.70782 for sanidine in OD). Feldspar rims are more radiogenic than the cores and bulk separates (0.70698 compared to 0.70686–0.70691 in OD plagioclase). Plagioclase overgrowths on sanidine are also significantly more radiogenic (OD sanidine = 0.70797 compared to 0.70772) despite having a lower Rb/Sr ratio comparable to that of the plagioclase separates. Large core-to-rim isotopic disequilibria are also found in sanidines from samples OL and OC (e.g., 0.715–0.720 and 0.7127–0.7202). All the quartz separates have low absolute Rb and Sr contents. The feldspar-bearing quartz has relatively low Rb/Sr compared to the host glass, whereas the quartz separate that contains melt inclusions has Rb/Sr and $^{87}Sr/^{86}Sr$ ratios higher than the host glass.

5.4. Pb and Nd isotope compositions

Pb and Nd isotope data are presented in Table 4 for samples OC, OD and OL, complementing fourteen Nd and nine Pb isotope analyses reported previously [4]. A striking feature of these results is the good agreement between all the data. There are no Nd and Pb isotope disequilibria between different phases within a sample, providing unequivocal evidence against late crustal contamination (Table 4).

Table 4
Mineral Nd and Pb isotope ratios

Sample	$^{143}Nd/^{144}Nd$	$^{206}Pb/^{204}Pb$	$^{207}Pb/^{204}Pb$	$^{208}Pb/^{204}Pb$
OD glass[1]	0.512467±16	19.163	15.695	39.007
OD whole rock[1]	0.512476±14	19.146	15.679	38.927
OD sanidine[1]	0.512494±17	19.148	15.661	38.888
OD plagioclase	0.512467±10	19.145	15.670	38.905
OD sanidine	0.512469±9	19.157	15.672	38.920
OD biotite >250 mm	0.512475±8	19.144	15.665	38.913
OD Fe-Ti oxides	0.512471±8			
OC glass[1]	0.512438±13	19.157	15.689	38.975
OC glass	0.512449±8	19.150	15.672	38.925
OC whole rock[1]	0.512455±17	19.146	15.679	38.977
OC sanidine	0.512454±10	19.153	15.680	38.932
OC plagioclase	0.512446±9	19.147	15.672	38.917
OC biotite >350 mm	0.512452±8	19.159	15.675	38.925
OC Fe-Ti oxides	0.512447±9			
OL whole rock[1]	0.512481±15	19.154	15.682	38.980
OL sanidine[1]	0.512484±25			
OL glass	0.512467±8	19.158	15.675	38.931
OL plagioclase	0.512474±8	19.147	15.679	38.924
OL sanidine	0.512462±9	19.152	15.665	38.919
OL Fe-Ti oxides	0.512473±8			

The centre of a 1 × 2 cm xenolith from OL has the following Sr-Nd isotope composition: $^{87}Sr/^{86}Sr = 0.710805 \pm 10$, $^{143}Nd/^{144}Nd = 0.512057 \pm 9$. Elemental concentrations (ppm): Rb = 45.3, Sr = 237.7 ($^{87}Rb/^{86}Sr = 0.55$); Sm = 3.52, Nd = 17.57 ($^{147}Sm/^{144}Nd = 0.121$) [1]From Halliday et al. [4].

5.5. Rb-Sr isochron ages

Lavas closest to the caldera margin (see Fig. 1) define a Rb-Sr isochron of 2.049 ± 0.013 Ma. Omitting whole-rock sample OD, which records petrographic evidence of minor hydration, reduces the MSWD from 21.8 to 11.1 with little effect on the isochron age (2.047 ± 0.013 Ma, Fig. 3A). These new data obtained on hand-picked glass are within error of the whole-rock Rb-Sr isochron age determined previously [4] (2.09 ± 0.06 Ma), confirming that the lavas have suffered little post-eruption alteration. Lavas more distant from the caldera wall define a Rb-Sr isochron age of 1.894 ± 0.013 Ma with a MSWD of 2.3 (Fig. 3B), within error of that determined previously [4] (1.90 ± 0.02 Ma). Initial ratios for the two suites are indistinguishable ($^{87}Sr/^{86}Sr = 0.7063 \pm 2$ and 0.7062 ± 2), which, coupled with comparable Nd and Pb isotope compositions, implies a similar origin. If the two rhyolite suites are derived from the same source the initial Sr ratios constrain the Rb/Sr ratio of that source to be $< 80 \pm 14$ even though lavas with Rb/Sr > 3000 were produced. The dividing line between inner and outer lavas trends NW–SE and is subparallel to the regional trend of the Sierran frontal escarpment fault and basement faults in the Long Valley region [16], possibly implying tectonic control in the formation of high-level magma reservoirs (Fig. 1).

6. Discussion

6.1. Phenocryst–melt isotopic equilibration

These data confirm the original observation made by Halliday et al. [4] that, despite being erupted over several hundred thousand years, the Glass Mountain rhyolites record Rb-Sr isochron ages that are significantly older than the time of rhyolite eruption. The question now is whether these data can be used to distinguish between remelting of recently crystallised magmas [10,11] and long magma residence times [4,12]. The fundamental difference between the two models is the length of time that the phenocryst populations have been in contact with a hot magma.

The origin of the minerals is fundamental to the interpretation of the Rb-Sr isotope data; i.e., do they represent phenocrysts, xenocrysts or a combination of both? The Nd and Pb isotope ratios of the basement and local sediments are

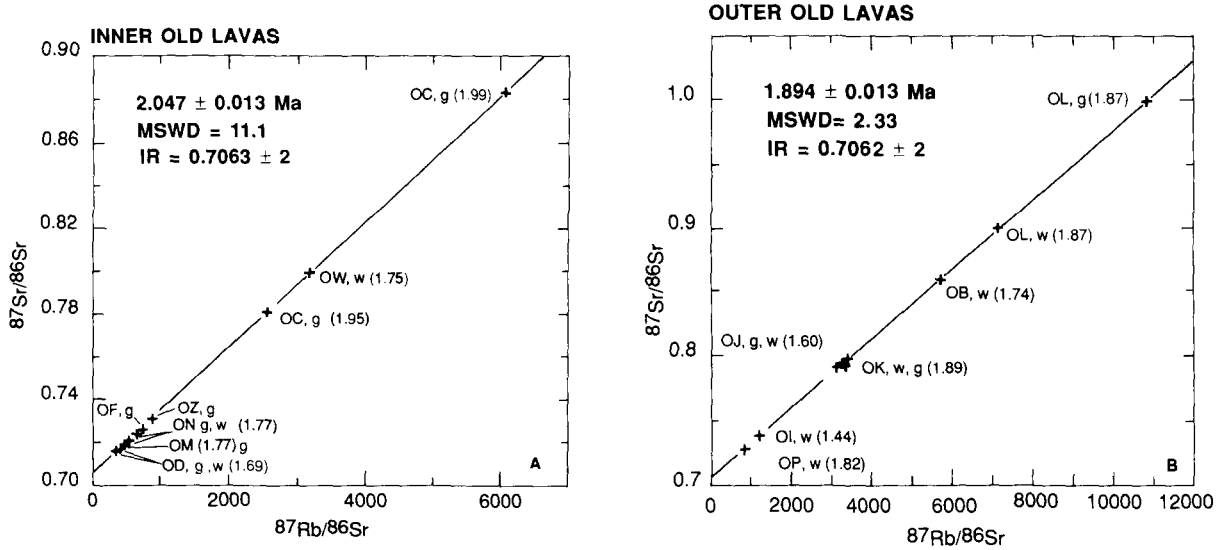

Fig. 3. Rb-Sr isotope diagrams for (A) Inner Lavas and (B) Outer Lavas. Ages in parentheses are eruption ages determined from K-Ar and Ar-Ar ages (g = glass; w = whole rock).

heterogeneous, with many rocks having isotopic compositions distinct from those of the Glass Mountain rhyolites (e.g., $^{206}Pb/^{204}Pb$ = ca. 18.5–20, $\epsilon_{Nd} = +6.5$ to -18, [17–23]). A small (1×2 cm) xenolith of basement material found in rhyolite OL confirms the isotopic difference of the basement (Table 4). Sampling of the mineral populations was biased by careful hand-picking such that any mineral thought to be from the very sparse xenocrystic population in OC and OL [8] has been removed. The success of the mineral picking has been confirmed by microprobe analyses of 50 representative grains from OD. Minerals from Glass Mountain lavas have Nd and Pb isotope ratios that are indistinguishable from their host glasses (Table 4), which again argues against the presence of a xenocryst population derived from the basement. Similarly, the single grain laser fusion ^{40}Ar-^{39}Ar ages are indistinguishable from corresponding bulk step-heating runs, implying that the sanidine samples represent a homogeneous population (Table 1). Therefore, with the possible exception of the excluded sparse xenocrysts, the phenocrysts in the Glass Mountain lavas are not derived from the basement. The Nd-Pb-Ar isotope data do not, however, preclude a xenocrystic contribution from older crystallised Glass Mountain magmas.

In the remelting and defrosting models [10,11] minerals represent material that either crystallised following the remelting or survived the remelting event and then underwent a period of re-equilibration with the host. In the long magma residence model phenocrysts could be in contact with a melt for up to 360 ka. The Rb-Sr systematics of a phenocryst suspended in melt will reflect a combination of the growth of radiogenic ^{87}Sr since its formation and diffusive re-equilibration between the mineral and host melt during residence in a magma chamber. Strontium diffusion in sanidine may be an order of magnitude faster under hydrous conditions than anhydrous conditions [24–26]. Sr diffusion in anorthite is an order of magnitude slower than in sanidine and orthoclase [26]. Baker [27] has shown that across an interface between very different silicate melts tracer (or self-) diffusion for Sr is faster than volume diffusion by approximately one order of magnitude. However, where the major element concentration gradient is low (e.g., within an unzoned silicate mineral or melt) tracer and volume diffusion are comparable [28]. The Sr feldspar diffusion data discussed above [24–26] are therefore a good analogue for the equilibration of $^{87}Sr/^{86}Sr$. Fe-Ti oxide temperatures obtained from Glass Mountain obsidians are ca. 700°C, similar to estimates for the early eruptive units of the Bishop Tuff [8,29]. At these temperatures, the estimated diffusion coefficient for sanidine is $\sim 10^{-17}$ cm^2/s and $\sim 10^{-18}$ cm^2/s for anorthite [25,26].

Following Crank [30] and Christensen and Delaolo [5], the degree of 'effective equilibration' between a 0.5 cm radius sphere and an enclosing magma as a function of diffusivity has been calculated for different residence times. By 'effective equilibration' we mean the amount of Sr that has exchanged between the melt and the mineral. This can be expressed as the change in $^{87}Sr/^{86}Sr$ of the crystal (i.e., average $^{87}Sr/^{86}Sr$ of the crystal at time t minus the initial $^{87}Sr/^{86}Sr$ of the crystal) divided by the difference between the initial $^{87}Sr/^{86}Sr$ ratios of the crystal and melt. For the estimated Sr diffusivity of the feldspars, it is apparent that the sanidine and plagioclase grains will undergo $< 5\%$ 'effective equilibration' over periods of up to 1 Ma. Total Sr isotope equilibration for plagioclase grains as small as 1 mm in radius would take more than 100 Ma. The greater the change in $^{87}Sr/^{86}Sr$ by radiogenic growth per unit time, the greater the Sr isotope disequilibrium between a crystal and a host magma. A 0.5 cm radius sphere that undergoes 5% 'effective equilibration' in 1.0 Ma will undergo only 3% 'effective equilibration' in a magma with a $^{87}Rb/^{86}Sr$ of 10,000 over the same period of time. The rhyolites have minimum melt compositions and should have formed at relatively low temperatures (< 750°C) [8]. Any feldspars that grew at time t_0 and survived a remelting event at t_1 would only undergo limited Sr re-equilibration with their host magmas if the time between remelting (at t_1) and eruption (at t_2) were short. Rapid re-equilibration at higher temperatures can be ruled out because this would melt the entire source rock. If the Glass Mountain rhyolites

formed by such remelting, all parts of unequilibrated individual feldspar grains, except any late rims that grew between t_1 and t_2, should lie on a mixing line between the core and the liquid on a Rb-Sr isochron diagram. Late rims would plot off this line and initially record the Sr isotopic composition of the liquid at the time of precipitation. Protracted feldspar growth and partial re-equilibration in a long-lived magma reservoir would result in the main portions of the feldspars yielding mixed data that plot neither toward the glass nor the late overgrowth. The Sr isotope data for sanidine and plagioclase separates from samples OC, OD and OL are presented in Table 3 and data for OD are presented graphically in Fig. 4. All feldspar composites and individual grain samples excluded material that contained thin translucent rims composed of plagioclase. However, the overgrowth was sampled during the microdrilling ('rim' in the diagrams). The feldspar populations plot above the regional isochrons (initial ratio of 0.7063 ± 2) and form slopes that are steeper than the isochrons. Plagioclases from OD define a slope equivalent to $\sim 31 \pm 5$ Ma whereas the sanidines define a slope of $\sim 3 \pm 1$ Ma (Fig. 4). The rims of plagioclase and sanidine do not lie on these regression lines. The Sr isotope systematics are consistent with the rims having formed in a later crystallisation event, at a time close to the eruption age. However, the bulk of the feldspars either formed over a long period of time or suffered significant isotopic exchange with the host magma prior to formation of the rims. Either way, this feature is most easily ex-

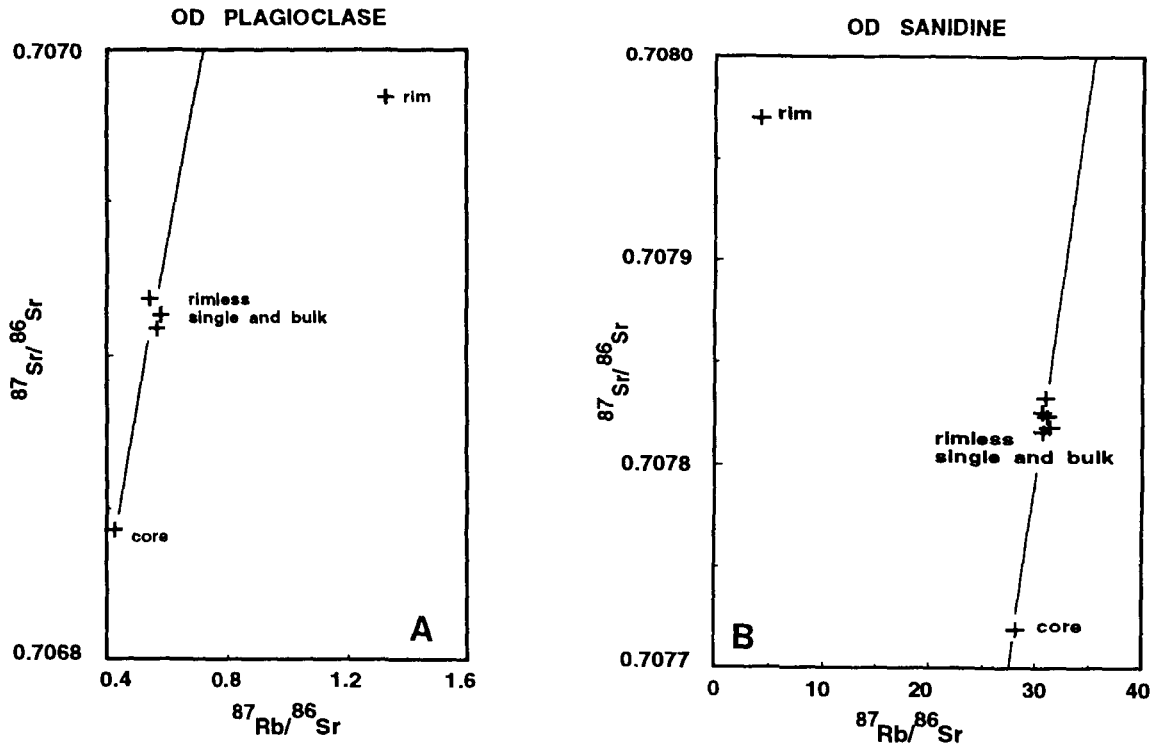

Fig. 4. Rb-Sr isotope diagram depicting feldspar data from sample OD. (A) Plagioclase. (B) Sanidine. All data lie above the regional isochron, which has an initial ratio of 0.7063 ± 2 such that the isochron lies well below the field defined by these diagrams. The regression lines on both figures are defined by grains without overgrowths and have a slope steeper than that of the regional isochron. These samples have Sr isotope systematics distinct from the overgrowths.

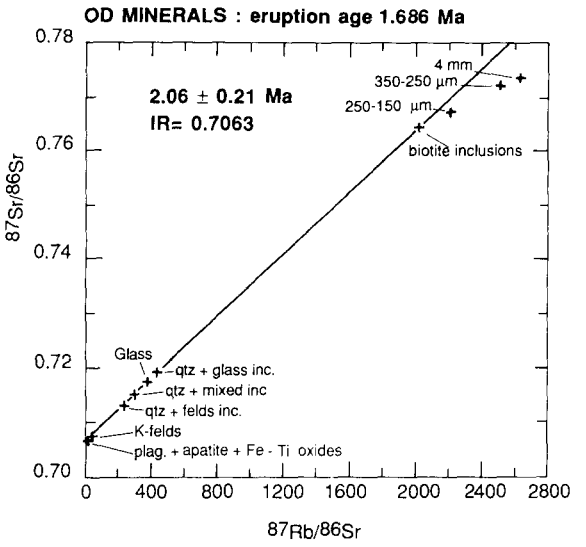

Fig. 5. Rb-Sr isotope diagram for the minerals from lava OD.

plained if the grains resided in a magma for a significant period of time and cannot be so readily explained by the remelting models [10,11].

6.2. Crystallisation ages of the minerals

The glass and bulk mineral separates of OD, excluding the biotite fractions, define a slope on a Rb-Sr isochron diagram equivalent to an age of 2.06 ± 0.21 Ma (Fig. 5). Conventionally, these data would be interpreted as the cooling age of the rock following eruption. However, the sanidine and biotite ^{40}Ar-^{39}Ar ages (1.686 ± 0.011 and 1.688 ± 0.038 Ma) are significantly younger, precluding such an interpretation. Sample OD lies on the 2.047 Ma regional glass isochron of the Inner Lavas and the mineral 'isochron' is within error of this age.

The Rb-Sr glass isochrons of the Glass Mountain Older Lavas record the timing of a marked fractionation in Rb/Sr. The low Sr contents and high Rb/Sr ratios of the rhyolites cannot be generated by crustal melting and require the extensive fractionation of a mineral with a high Sr K_d such as feldspar [12,31]. Even if a subsequent remelting model is accepted the Rb-Sr isochrons represent an earlier major chemical differentiation event during the evolution of the rhyolites when Rb/Sr ratios were fractionated. The precision of the regional Rb-Sr isochrons implies that this was completed in less than 26 ka (Fig. 3).

The diffusion modelling establishes that the cores of large sanidine and plagioclase phenocrysts will retain > 99.9% of the Sr initially present at the time of crystallisation, even after 1.0 Ma of residence in a magma. Consequently, if the Rb/Sr ratios of the melts do not significantly change during residence in the chamber, glass–feldspar core ages should define the time of crystal growth. The viscosity of the rhyolites and their low phenocryst population, coupled with preservation of the regional isochrons, enables us to

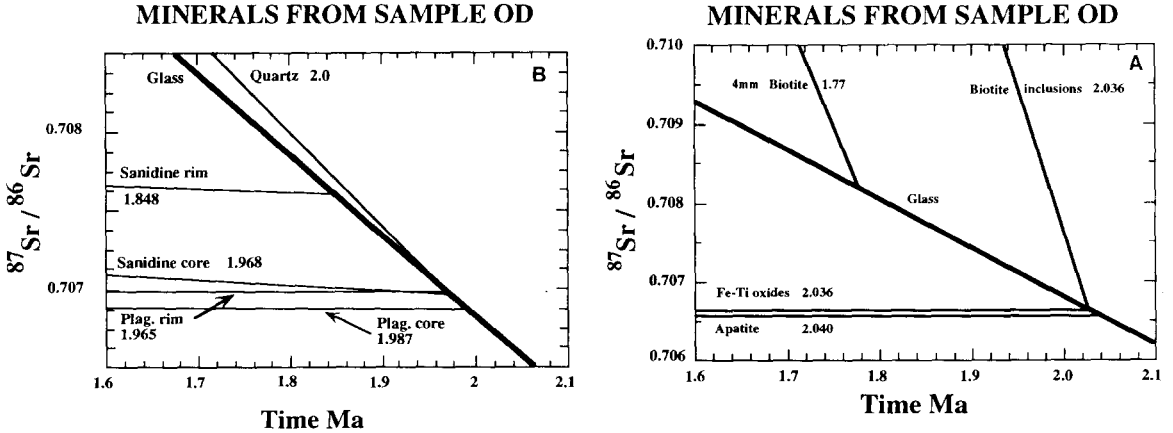

Fig. 6. Sr isotope evolution diagram for minerals from Glass Mountain lavas. (A) Early crystallised phases from sample OD. The eruption age of OD is 1.686 ± 0.011 Ma. (B) Later crystallised phases from sample OD.

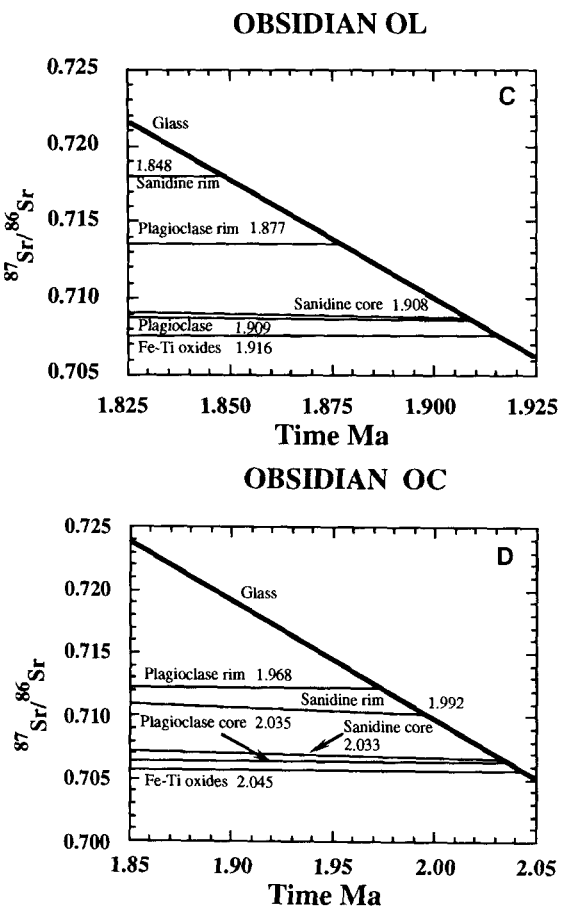

Fig. 6. (C) Minerals from sample OL with eruption age of 1.990 ± 0.012 Ma. (D) Minerals from sample OC with eruption age of 1.867 ± 0.005 Ma.

argue that the Rb/Sr ratios of the magmas cannot have been further modified by extensive crystallisation.

Glass–mineral ages (hereafter referred to as mineral ages) are presented in Table 3 and graphically in Fig. 6. A partial derivative analysis of the error in the age difference between two phases (e.g., $t_{\text{plagioclase}} - t_{\text{sanidine}}$) demonstrates that the contribution from the analytical error of the glass is minor. The error in the age difference between minerals from a single sample is dominated by the analyses of the mineral phases. Errors in the age differences between two phases are below 1 ka for samples OC and OL, which have the highest glass Rb/Sr (Table 5). Feldspar core ages from samples OC and OL are within error of the regional isochrons whereas the feldspar core ages from sample OD are younger but only just outside analytical uncertainty (Fig. 3 and Table 3).

Apatite, Fe-Ti oxide and biotite, which occur as inclusions in quartz and feldspar, crystallised before the bulk of the feldspar population. Fe-Ti oxide ages for all three samples are within error of the regional isochrons. Ages from the biotite inclusions from sample OD are older than the feldspar cores and again within error of the regional isochron (Figs. 6A and B). These older ages imply that the feldspars and quartz have effectively armoured the biotite and prevented equilibration with the magma. The apatite composites extracted from the biotite of sample OD record the oldest ages from this sample (Fig. 6A). Experimental studies of Sr diffusion in apatite have established that Sr diffusion is slow, of the order of 10^{-18} cm^2/s [32–34]. The calculated closure temperature for Sr in a 1 mm apatite grain is ~ 700°C assuming a cooling rate between 10 and 1000°C/Ma, which is probably applicable for the Long Valley magma chamber(s) [32–34]. The apatite inclusions obtained from OD biotite phenocrysts retain the oldest mineral age, implying that the blocking temperature for apatite is as high as previously inferred [32–34] or that the biotite host has effectively armoured the apatite inclusions.

There is a perfect correspondence between the mineral ages and the order of crystallisation deduced from inclusion relationships (Fig. 6). These data are fully consistent with gradual crystallisation from a magma. There is no rationale in a remelting model that predicts these relationships. The sanidine and plagioclase cores from sample OD yield ages that are ca. 50 ka younger than the mineral thought to crystallise first. Plagioclase is older than sanidine, consistent with the inclusion relationships. Samples OC and OL have the same relative age relationships: the age of the bulk plagioclase separates are older than sanidine (Figs. 6C and D). Quartz consistently yields the youngest age but, due to the similar Rb/Sr ratios between quartz and host glass, the error in the age is relatively large. While these data cannot be explained by the defrosting model [11] the miner-

Table 5
Compilation of mineral ages

MINERAL PAIR	AGE Ma	AGE DIFFERENCE Kyrs
LAVA OD $T_{regional}$ = 2.047 ± 0.013 Ma; $T_{erupt.}$ = 1.686 ± 0.011 Ma		
Apatite	2.0404	
Fe-Ti oxides	2.0363	4 ± 3
Fe-Ti oxides	2.0363	
Biotite inclusions	2.0356	0.7 ± 18
Biotite inclusions	2.0356	
Plagioclase core	1.9875	48 ± 18
Plagioclase core	1.9875	
Sanidine core	1.9676	20 ± 4
Plagioclase core	1.9875	
Plagioclase rim	1.9654	22 ± 4
Sanidine core	1.9676	
Sanidine rim	1.7906	177 ± 4
LAVA OC $T_{regional}$ = 2.047 ± 0.013 Ma; $T_{erupt.}$ = 1.990 ± 0.011 Ma		
Fe-Ti oxides	2.0453	
Plagioclase core	2.0350	9.7 ± 0.5
Plagioclase core	2.0350	
Sanidine core	2.0328	2.7 ± 0.5
Plagioclase core	2.0350	
Plagioclase rim	1.9677	67.3 ± 0.4
Sanidine core	2.0328	
Sanidine rim	1.9922	40.6 ± 0.7
LAVA OL $T_{regional}$ = 1.894 ± 0.013 Ma; $T_{erupt.}$ = 1.866 ± 0.014 Ma		
Fe-Ti oxides	1.9161	
Plagioclase	1.9093	6.8 ± 0.1
Plagioclase	1.9093	
Sanidine core	1.9081	1.2 ± 0.3
Plagioclase	1.9093	
Plagioclase rim	1.8770	32.3 ± 0.2
Sanidine core	1.9081	
Sanidine rim	1.8480	60.1 ± 0.6

als could have had a long magma residence time prior to solidification and subsequent remelting, provided the Rb-Sr isotope systematics of the minerals were not disrupted by the remelting. In this case these data can still be used to infer the early crystallisation history of the magmas.

The time from apatite crystallisation to the initiation of sanidine crystallisation is 72 ± 3 ka for sample OD (Fig. 6A and B). The earliest dated phase to crystallise in OL and OC is Fe-Ti oxide. The time between Fe-Ti oxide crystallisation and initiation of sanidine crystallisation is 12.4 ± 0.6 ka for OC and 8.0 ± 0.3 ka for OL (Figs. 6C and D). The age differences between plagioclase and sanidine cores show the same relative chronology: for OD 19.8 ± 3.8 ka, for OC 2.8 ± 0.5 ka, and for OL 1.2 ± 0.3 ka. Lava OD is the most crystal rich and least evolved, displays the longest time difference between differentiation and eruption, and displays the slowest crystallisation rates. These relationships imply that the chemically more evolved samples (i.e., those with greater Rb/Sr ratios) had shorter crystallisation histories, cooled more rapidly and were more liable to extrusion, possibly implying that they resided at shallower levels in a magma chamber. Note that these relationships are not readily predicted by the remelting models.

The maximum magma chamber residence for minerals from sample OD is 361 ka (regional isochron age minus eruption age from 2.047 to 1.686 Ma). In this time period the $^{87}Sr/^{86}Sr$ of the magma would increase by 0.00189. The differences in $^{87}Sr/^{86}Sr$ ratios at 1.686 Ma ($^{87}Sr/^{86}Sr_e$) between core and bulk compositions for both sanidine and plagioclase are outside analytical uncertainty (0.00007 ± 4, Table 3). In 360 ka a 5 mm radius feldspar grain would undergo a maximum of 1% equilibration with the host magma (i.e., a change in $^{87}Sr/^{86}Sr$ ratios of 0.00002, close to the observed variation of 0.00007 ± 4). In contrast, the data from sample OL, which has the highest Rb/Sr ratio and hence most rapid change in $^{87}Sr/^{86}Sr$, are incompatible with significant

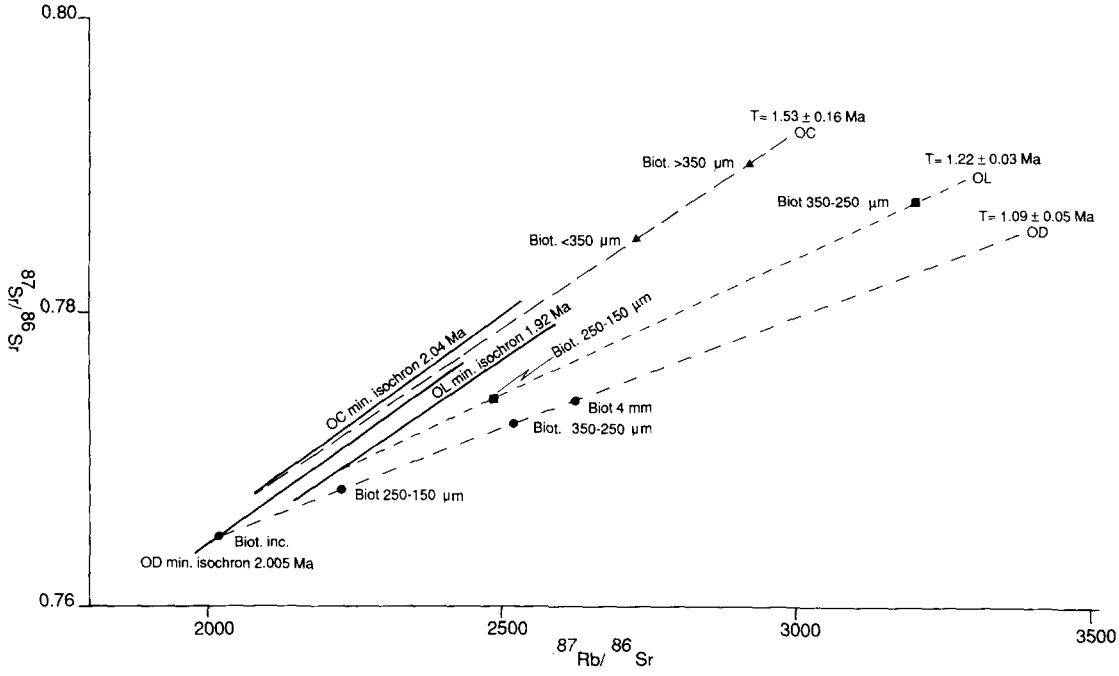

Fig. 7. Rb-Sr isotope diagram depicting the position of different biotite size fractions in relation to the mineral isochrons defined by plagioclase, sanidine, Fe-Ti oxide, quartz and glass for samples OD, OC and OL. In all cases biotite populations plot below the mineral isochrons even though the $^{87}Sr/^{86}Sr$ ratio of the host glasses varies from significantly less radiogenic than the biotites (OD) to more radiogenic (OC and OL). See text for further discussion.

re-equilibration. The difference in $^{87}Sr/^{86}Sr_e$ ratios between core and bulk sanidine compositions is 0.0033. The maximum time difference between eruption of OL (1.866 ± 0.14 Ma) and the regional isochron (1.893 ± 0.013) is 54 ka. In this time the $^{87}Sr/^{86}Sr$ of the magma would increase by 0.0083. However, in such a short time little Sr isotope re-equilibration would occur between the magma and minerals ($< 0.1\%$), suggesting that the bulk and single grain mineral data are recording variations in the time of mineral formation.

The translucent rims of both plagioclase and sanidine from OL and OC yield Rb-Sr ages within error of their respective eruption ages. The rims were sampled by microdrill and probably represent a mixture of the thin (0.1 mm) overgrowth and a minor portion (probably close to 15%) of the interior. The estimated residence times for the feldspar of samples OL and OC are 60.1 and 67.3 ka respectively (core ages minus eruption age, Table 5). Diffusion calculations show that the outer 0.2 mm of a 5 mm radius grain would undergo ca. 20% Sr equilibration in 100 ka assuming a diffusivity of Sr of 10^{-17} cm^2/s and a moderate increase in radiogenic ^{87}Sr ($^{87}Rb/^{86}Sr = 1000$). The short residence times of feldspar in samples OL and OC demonstrate that the rim ages cannot be interpreted entirely in terms of equilibration. This conclusion is confirmed by the sanidine rim from sample OD which gives an age that is 177 ka younger than the core and 105 ka older than the age of eruption. If considered simply in terms of re-equilibration, these age relationships would imply ca. 60% equilibration between the mineral and magma, far too large to ascribe simply to diffusive processes. Given the rapid change in $^{87}Sr/^{86}Sr$ with time and the short residence times for samples OC and OL it can be concluded that the feldspar rims in these samples grew at a time indistinguishable from that corresponding to the eruption age. Hence, it can be also concluded that plagioclase and sanidine growth occurred over periods of 30–60 ka in sample OL and 67–40 ka in sample OC. Due to the effects of re-equilibration, the 177 ka difference between sanidine core and rim ages of sample OD is probably an over-estimate by between 5 and 15%, depending on the true residence time. The $t_{core} - t_{rim}$ for plagioclase from OD is only 22 ka, which represents 7% of the plagioclase residence time. This is indistinguishable from the calculated degree of equilibration in 300 ka. Within an individual sample, ages obtained from cores, composite separates and individual grains from both sanidine and plagioclase are similar (Table 4). Therefore the bulk of the feldspar crystallisation was probably rapid (< 15 ka).

6.3. Biotite Rb-Sr isotope systematics

Currently there are on;y limited Sr diffusion data for biotite [35,36]. K and Rb data [35] suggest diffusivities of ca. 10^{-13} cm^2/s at the magmatic temperatures of the Glass Mountain rhyolites. Providing that Sr and Rb diffusion in biotite are not more than several orders of magnitude different and even accounting for the rapid changes in the $^{87}Sr/^{86}Sr$ ratio of the melt, a 1 cm long biotite xenocryst would undergo almost total equilibration with a magma in < 25 ka. The different size biotite populations from OD yield mineral ages ($1.90–1.77 \pm 0.01$ Ma) that are younger than the regional glass isochron age of 2.047 ± 0.013 Ma, but older than the eruption age 1.676 ± 0.011 Ma. In contrast, the biotite inclusion composite separated from quartz and feldspar yields an age of 2.036 ± 0.013 Ma, indistinguishable from the regional isochron but 48 ka older than the plagioclase core. Biotite composites from samples OC and OL were also in Sr isotope disequilibrium with their host at the time of eruption (Fig. 7). Biotite fractions from all three samples have high Rb/Sr ratios (ca. 1000) and plot below the regional glass isochrons on the Rb-Sr isochron diagram, demonstrating that these populations contain little, if any, xenocrystic material from the country rocks. Biotite–glass ages for samples OC and OL are older than the regional isochrons due to the biotites having lower Rb/Sr ratios than the glass and plotting below the isochrons. The coarsest biotite size fraction of sample OD gives the youngest apparent age (1.765 ± 0.010 Ma). Diffusion-controlled processes would produce the opposite relationship, with smaller grains undergoing the greatest iso-

topic exchange. The different biotite size fractions of OD define a mixing relationship on a Rb-Sr isochron diagram (Fig. 7). Biotites from samples OL and OC are also discordant from their respective mineral isochrons, with the coarser grain size fractions the most discordant. The relationships defined by all three biotite populations can be interpreted in terms of mixing between biotite inclusions armoured by quartz or feldspar and larger phenocrysts that have undergone isotopic exchange with the magma and/or grown later. Smaller biotite size fractions are interpreted to contain a greater proportion of biotite inclusions liberated from host quartz and feldspar grains during sample crushing. A mineral with lower Rb/Sr and $^{87}Sr/^{86}Sr$ ratios than the host magma which undergoes Sr isotope exchange with the magma results in a mineral with increased $^{87}Sr/^{86}Sr$ ratios that plots above the mineral isochron. Despite having lower $^{87}Sr/^{86}Sr$ and Rb/Sr than their host lava, the biotites of samples OL and OC do not show this relationship. Similarly, the larger biotite size fractions of OD have increased Rb/Sr and $^{87}Sr/^{86}Sr$ ratios compared to the biotite inclusion population, causing them to plot below the mineral isochrons. These data can be explained if the Rb/Sr ratio of the biotite increases after crystallisation by partial re-equilibration with the melt. For this model to be valid the Rb/Sr ratio of the liquid or the equilibrium partition coefficient must change after crystallisation of the biotite. A more likely explanation is that the larger biotites represent xenocrysts from earlier crystallised Glass Mountain rhyolites elsewhere in the magma chamber. This would help explain the similar Rb/Sr ratios of the biotites irrespective of the host glass Rb/Sr ratio and the small amounts of excess Ar found in the biotites from OD. However, mixing of material between different levels of the magma chamber must have been limited in order to preserve the regional Rb-Sr isochron.

6.4. Mineral growth rates

Current estimates of magma crystallisation rates come principally from studies of rapidly cooling 'basaltic systems' [6]. Minimum mineral growth rates for the Glass Mountain rhyolites can be calculated by assuming that grains grew over the entire period of residence in the magma chamber. The growth rates calculated below are average linear growth rates and are not intended to obscure a more complex history of mineral growth that almost certainly occurred. The largest feldspar grains are up to 1 cm in diameter (i.e., 0.5 cm^3). Assuming a maximum residence time of 360 ka for sample OD and 32 ka for OL yields growth rates of between 1.4×10^{-6} and 8.7×10^{-5} cm^3/yr. The mineral Sr isotope systematics indicate, however, that growth rates were faster. The plagioclase in sample OD grew in significantly less time than 22 ka (the maximum age difference between core and rim assuming no effects from diffusion), which implies an average growth rate of 2.4×10^{-5} cm^3/yr. This equates to a linear growth rate of 7.2×10^{-13} cm/s. The extent to which mineral growth was continuous or episodic is unknown, but large differences between the feldspar rim ages and the eruption age of sample OD implies that crystallisation stopped long before eruption. Coupled with the fact that feldspar cores and bulk grains yield similar ages and the presence of the thin plagioclase overgrowths on sanidine grains, these observations are indicative of episodic growth, which imply that faster growth rates operated at least periodically, but we are unable to constrain maximum growth rates.

Growth rates can also be determined from inclusion relationships. Plagioclase crystals are found forming the nucleus of sanidine grains in all three samples. The time difference between the formation of plagioclase and sanidine cores is 19.8 ± 3.8 ka for sample OD and 2.7 ± 0.5 ka for sample OC. The size of the plagioclase inclusions was determined from the largest sanidine grains, which are assumed to have been the first sanidines to begin crystallising. The largest plagioclase inclusions are 0.1 cm long, and they must have grown before the onset of sanidine growth. This implies a linear growth rate of $5.9 \pm 1.1 \times 10^{-13}$ cm/s for sample OC and $8.0 \pm 1.3 \times 10^{-14}$ cm/s for OD, similar to estimates for the Bishop Toff [5]. The faster growth rate would produce a feldspar 11 cm in diameter in the 300 ka resi-

dence time of plagioclase in sample OD, demonstrating that feldspar crystallisation was not continuous in the magma system over the entire magmatic history of the lavas.

6.5. Magma production rates

The Rb/Sr ratios of up to 3600 at Glass Mountain require that a parental magma with 100 ppm Sr (typical value for crustal melts) undergoes $>99\%$ fractionation of an assemblage with a bulk Sr K_d of >2 (i.e., dominated by sanidine and plagioclase [31]). It is impossible that the observed sparse phenocryst population at Glass Mountain was responsible for magma differentiation. The volume of the entire magma system is unknown due to disruption by caldera formation. The total amount of pre-1.2 Ma lavas present today is >20 km^3, which places a lower limit on the size of the magma chambers [8]. The fact that the Older Lavas lie on regional isochrons with precisions of $\pm 13{,}000$ yr implies that the precursor to the silicic magma differentiated rapidly and produced high-silica rhyolite at a rate of at least 0.8×10^{-3} km^3/yr.

Eruption of Glass Mountain lavas terminated with eruption of the Bishop Tuff and the formation of the Long Valley Caldera. Isotopic similarities between post-1.2 Ma lavas and the Bishop Tuff [9] imply derivation from the same magma and hence that >700 km^3 of magma was produced between ca. 1.1 and 0.74 Ma. This would imply a production rate of 1.9×10^{-3} km^3/yr, comparable to the estimate made by Christensen and DePaolo [5]. However, the post-1.2 Ma lavas also define regional isochrons (e.g., 1.151 ± 0.010 Ma [37]), demonstrating a rapid differentiation process. If the Bishop Tuff magma were produced in these events a production rate of 3.5×10^{-2} km^3/yr is implied.

Previous estimates of the production rate of silicic magma systems have been based on the relationships between eruptive volume and repose time [1]. Recent compilations conclude production rates are of the order of 10^{-2}–10^{-4} km^3/yr, with a mean of 10^{-3} km^3/yr [2]. The data presented here argue for magma production as an episodic rather than continuous process. Hence, the production rates of silicic systems determined in previous studies [1,2] may be too low and in reality are probably more comparable to basaltic systems than previously realised (e.g., 10^{-2} km^3/yr [38]).

Acknowledgements

This work was supported by National Science Foundation grants EAR 8915986, 9004133 and 9205435. We are grateful for assistance with TEM and microprobe analysis by E. Snow and C. Henderson. R. Keller and M. Johnston provided invaluable technical assistance. K. Mezger, D. Palais, S. Tommasini and R. Lange provided criticism of early versions of the manuscript. We thank Y. Zhang and B. Watson for discussion and access to their (then) unpublished data. Reviews by Richard Carlson, Jonathan Patchett and Stephen Blake are gratefully acknowledged too.

References

[1] R.L. Smith, Ash flow magmatism, Geol. Soc. Am. Spec. Pap. 180, 5–26, 1979.
[2] F.J. Spera and J.A. Crisp, Eruption volume, periodicity and caldera area: relationships and inferences on development of compositional zonation in silicic magma chambers, J. Volcanol. Geotherm. Res. 11, 169–187, 1981.
[3] B. Marsh, Magmatic processes, Rev. Geophys. 25, 1043–1053, 1987.
[4] A.N. Halliday, G.A. Mahood, P. Holden, J.M. Metz, T.J. Dempster and J.P. Davidson, Evidence for long residence times of rhyolitic magma in the Long Valley magmatic system: the isotopic record in precaldera lavas of Glass Mountain, Earth Planet. Sci. Lett. 94, 274–290, 1989.
[5] J.N. Christensen and D.J. DePaolo, Timescale of large volume silicic magma systems: Sr isotopic systematics of phenocrysts and glass from the Bishop Tuff, Long Valley, California, Contrib. Mineral. Petrol. 113, 100–114, 1993.
[6] K.V. Cashman, Textural constraints on the kinetics of crystallization of igneous rocks, in: Modern Methods of Igneous Petrology, J. Nicholls and J.K. Russell, eds., Mineral. Soc. Am. Spec. Publ. 24, 259–314, 1991.
[7] J.M. Metz and G.A. Mahood, Precursors to the Bishop Tuff eruption, Glass Mountain, Long Valley, California, J. Geophys. Res. 90, 11121–11126, 1985.
[8] J.M. Metz and G.A. Mahood, Development of the Long Valley, California magma chamber recorded in precaldera rhyolite lavas of Glass Mountain, Contrib. Mineral. Petrol. 106, 379–397, 1991.
[9] A.N. Halliday, A.E. Fallick, J. Hutchinson and W. Hildreth, A Nd, Sr and O isotopic investigation into the

causes of chemical and isotopic zonation in the Bishop Tuff, California. Earth Planet. Sci. Lett. 68, 379–391, 1984.
[10] R.S.J. Sparks, H.E. Huppert and C.J.N. Wilson, Comment on 'Evidence for long residence times of rhyolitic magma in the Long Valley magmatic system: the isotopic record in precaldera lavas of Glass Mountain' by Halliday A.N., Mahood G.A., Holden P., Metz J.M., Dempster, T.J. and Davidson J.P., Earth Planet. Sci. Lett. 99, 387–389, 1991.
[11] G.A. Mahood, Second reply to comment of Sparks R.S.J., Huppert H.E. and Wilson C.J.N. on 'Evidence for long residence times of rhyolitic magma in the Long Valley magmatic system: the isotopic record in precaldera lavas of Glass Mountain', Earth Planet. Sci. Lett. 99, 395–399, 1991.
[12] A.N. Halliday, Reply to comment of Sparks R.S.J., Huppert H.E. and Wilson C.J.N. on 'Evidence for long residence times of rhyolitic magma in the Long Valley magmatic system: the isotopic record in precaldera lavas of Glass Mountain', Earth Planet. Sci. Lett. 99, 390–394, 1991.
[13] G.R. Davies, unpublished data.
[14] E. Snow, pers. commun.. 1991.
[15] Ph. Lo Bello, G. Féraud, C.M. Hall, D. York, P. Lavina and M. Bernat, ^{40}Ar-^{39}Ar step-heating and laser fusion dating of Quaternary volcanics from Neschers, Massif Central, France: The defeat of xenocrystal contamination, Chem. Geol. (Isot. Geosci. Sect.), 66, 61–71, 1987.
[16] C.M. Gilbert, M.N. Christensen, Y. Al-Rawi and K.R. Lajoie, Structural and volcanic History of Mono Basin, California–Nevada, Geol. Soc. Am. Mem. 116, 275–329, 1968.
[17] D.J. DePaolo, A neodynium and strontium isotopic study of the Mesozoic calc-alkaline granitic batholith of the Sierra Nevada and Peninsular ranges, California, J. Geophys. Res. 86, 10470–10488, 1981.
[18] R.A. Bailey, Geological map of the Long Valley caldera, Mono–Inyo–Craters volcanic chain, and vicinity, eastern California, U.S. Geol. Surv. Map I-1933, 1989.
[19] W.D. Sharp, Pre-Cretaceous crustal evolution in the Sierra Nevada region of California, in: Metamorphism and Crustal Evolution of the western United States, Rubey Vol. VII, W.G. Ernst, ed., pp. 823–864, Prentice-Hall, 1988.
[20] B.R. Doe and M.H. Delevaux, Variations in the lead-isotopic compositions in Mesozoic granitic rocks of California—a preliminary investigation, Geol. Soc. Am. Bull. 84, 3513–3526, 1973.
[21] M.A. Domenick, R.W. Kistler, F.C.W. Dodge and M. Tatsumoto, Nd and Sr isotopic study of crustal and mantle inclusions from the Sierra Nevada xenoliths and implications for batholith petrogenesis, Geol. Soc. Am. Bull. 94, 713–719, 1983.
[22] J.B. Saleeby et al., Corridor C-2, Central California offshore to Colorado plateau, centennial continent–ocean transect 10, Geol. Soc. Am., 1986.
[23] J.L. Wooden, J.S. Stacey, K.A. Howard, B.R. Doe and D.M. Miller, Pb isotopic evidence for the formation of Proterozoic crust in the southwestern United States, in: Metamorphism and Crustal Evolution of the western United States, Rubey Vol. VII, W.G. Ernst, ed., pp. 68–86, Prentice-Hall, 1988.
[24] E.B. Watson and D.J. Cherniak, Diffusion of strontium and rubidium in K-feldspar measured by Rutherford backscattering spectroscopy, EOS 72(17), 309, 1991.
[25] B.J. Giletti, Rb and Sr diffusion in alkali feldspar, with implications for cooling histories of rocks, Geochim. Cosmochim. Acta 55, 1331–1343, 1991.
[26] D.J. Cherniak and E.B. Watson, A study of strontium diffusion in K-feldspar, Na-K-feldspar and anorthite using Rutherford Backscattering Spectroscopy, Earth Planet. Sci. Lett. 113, 411–425, 1992.
[27] D.R. Baker, Tracer versus trace element diffusion: Diffusional decoupling of Sr concentration from Sr isotope composition, Geochim. Cosmochim. Acta 53, 3015–3023, 1989.
[28] S. van der Laan, Y. Xhang, A.K. Kennedy and P.J. Wyllie, Comparison of element and isotope diffusion of K and Ca in multicomponent silicate melts, Earth Planet. Sci. Lett. 123, 155–166, 1994.
[29] W. Hildreth, The Bishop Tuff: evidence for the origin of compositional zonation in silicic magma chambers, Geol Soc. Am. Spec. Pap., 180, 43–75, 1979.
[30] J. Crank, The Mathematics of Diffusion. Oxford University Press, 1975.
[31] A.N. Halliday, J.P. Davidson, W. Hildreth and P. Holden, Modelling the petrogenesis of high Rb/Sr silicic magmas, Chem. Geol. 92, 107–114, 1991.
[32] E.B. Watson, T.M. Harrison and F.J. Ryerson, Diffusion of Sm, Sr and Pb in fluorapatite, Geochim. Cosmochim. Acta 49, 1813–1823, 1985.
[33] J.R. Farver and B.J. Giletti, Oxygen and strontium diffusion kinetics in apatite and potential applications to thermal history determinations, Geochim. Cosmochim. Acta 53, 1621–1631, 1991.
[34] D.J. Cherniak and F.J. Ryerson, A study of strontium diffusion in apatite using Rutherford backscattering spectroscopy and ion implantation, Geochim. Cosmochim. Acta 57, 4653–4662, 1993.
[35] A.W. Hofmann, B.J. Giletti, J.R. Hinthorne, C.A. Anderson and D. Comaford, Ion microprobe analysis of a potassium self-diffusion experiment in biotite, Earth Planet. Sci. Lett. 24, 48–52, 1974.
[36] B.J. Giletti, Diffusion kinetics of Mg, Ca, Sr and Ba in albite and Sr in muscovite and biotite, EOS 72(44), 528, 1991.
[37] G.R. Davies, A.N. Halliday and G.A. Mahood, The crystallization ages of minerals from a silicic magma chamber, in: Proc. ICOG 7, p. 25, Geol. Soc. Aust. 27, 1990.
[38] H.R. Shaw, Links between magma–tectonic rate balances, plutonism and volcanism, J. Geophys. Res. 90, 11275–11288, 1985.
[39] J.M. Metz and R.A. Bailey, Geologic map of Glass Mountain, Long Valley, California, U.S. Geol. Surv. Map. I-1995.